Dense Gas Thermodynamic Properties of Single and Multicomponent Fluids for Fluid Dynamics Simulations

Piero Colonna
Faculty of Design, Engineering and Production,
Thermal Power Engineering Section,
Delft University of Technology,
Mekelweg 2,
2628 CD Delft, The Netherlands

Paolo Silva
Dipartimento di Energetica,
Politecnico di Milano,
P.za L. da Vinci, 32,
20133 Milano, Italy

The use of dense gases in many technological fields requires modern fluid dynamic solvers capable of treating the thermodynamic regions where the ideal gas approximation does not apply. Moreover, in some high molecular fluids, nonclassical fluid dynamic effects appearing in those regions could be exploited to obtain more efficient processes. This work presents the procedures for obtaining nonconventional thermodynamic properties needed by up to date computer flow solvers. Complex equations of state for pure fluids and mixtures are treated. Validation of sound speed estimates and calculations of the fundamental derivative of gas dynamics Γ *are shown for several fluids and particularly for Siloxanes, a class of fluids that can be used as working media in high-temperature organic Rankine cycles. Some of these fluids have negative* Γ *regions if thermodynamic properties are calculated with the implemented modified Peng-Robinson thermodynamic model. Results of flow simulations of one-dimensional channel and two-dimensional turbine cascades will be presented in upcoming publications.* [DOI: 10.1115/1.1567306]

1 Introduction

The study of fluid flows involving dense gases, i.e., fluids that cannot be treated as an ideal gas, is of particular interest for several applications. Examples are the hypersonic and transonic wind tunnel design, [1–4], chemicals and fluids transport, [5], heat transfer devices (especially in chemical processes), and supercritical hydrogen to cool hypersonic aircrafts, [6]. One area that can benefit from advances in the mentioned field is turbomachinery design, primarily organic Rankine cycle (ORC) turbines, [7,8], but also compressors and turboexpanders for chemical processes and compressors for refrigeration applications, [9,10]. Other areas which can involve dense gas dynamics are the development of Stirling engines, [11,12], and of thermoacoustic engines, [13].

So-called dense gas effects occur for thermodynamic states at high pressure close to saturation and close to the critical point. The volumetric effect implies that densities are smaller if compared to the ideal gas approximation and the calorimetric effect implies that the heat capacity close to the critical point tends to large values.

For an accurate numerical simulation of dense gas flows these effects must be accounted for and the use of complex thermodynamic models as opposed to the widely adopted ideal gas approximation is mandatory. The introduction of complex thermodynamic models into fluid dynamics numerical schemes is not straightforward, [14–19]; furthermore, modern solvers require the computation of particular thermodynamic functions for time-efficient and accurate implementation. An overview of the mentioned functions, procedures to obtain their algebraic expressions, and their form for several thermodynamic models are outlined in the following. The present study extends the previous work (see, e.g., Refs. [20–22]) regarding the use of complex equations of state (EOS) in fluid dynamic simulations to other accurate EOS and to state-of-the-art EOS for mixtures.

Besides dense gas behavior, nonclassical gasdynamic effects could also occur in the critical or near subcritical dense gas region and are extensively documented in the literature (see, e.g., Ref. [23] for a review and complete references, and also Refs. [24–28] for more recent works). Nonclassical dense gas behavior could be exploited in the design of ORC turbines or other turbomachinery to reduce losses related to shock formation, [7,9,10]. The thermodynamic parameter governing nonclassical behavior is the fundamental derivative of gas dynamics Γ.

Estimates of Γ values for siloxanes, a class of fluids recently proposed and adopted in ORC turbine applications, are also presented. The complete thermodynamic models which are illustrated in the following are implemented in a FORTRAN library, THERMOPROP. The thermodynamic library is part of ZFLOW, a computational fluid dynamics (CFD) Euler solver developed in collaboration by the authors and others, [29]. Results for nozzle, shock-tube, and cascade configurations will be presented in upcoming publications.

2 Thermodynamic Properties for Numerical Flow Solvers From Complex Equations of State

A Thermodynamic Models. Using a consistent model for the estimation of thermodynamic properties to be used in a fluid dynamics numerical solver is very important in order to achieve robustness and accuracy. This means that all needed thermodynamic properties must be computed from the minimum set of information, e.g., an EOS in the usual $P=P(v,T)$ form, where P is the pressure, T the temperature, and v the specific volume. The other necessary information is the heat capacity in the ideal gas state as a function of temperature, $C_P^0=C_P^0(T)$, [30].

Multi-parameter equations of state (MEOS) for the estimation of thermodynamic properties of both the liquid and the vapor phase are very accurate even in the closest proximity of the critical point, [31,32], while widely adopted cubic equations of state (CEOS) are inherently inaccurate near the critical point, [33], but need very limited input information and, more importantly, can be extended to multicomponents fluids on a thermodynamically consistent basis, [31,34].

MEOS can be substance-specific, like the modified Keenan-Keyes EOS for water, [30,35], or the Haar-Gallagher EOS for ammonia, [30,36], can fit a specific class of fluids, like the Star-

Contributed by the Fluids Engineering Division for publication in the JOURNAL OF FLUIDS ENGINEERING. Manuscript received by the Fluids Engineering Division May 28, 2002; revised manuscript received October 30, 2002. Associate Editor: J. Katz.

ling EOS for light hydrocarbons, [30,37], or can be used for various classes of substances with a comparably lower precision, like the Martin-Hou EOS, [30,38,39]. In order to give an overview of the accuracy of the above-cited models, the overall accuracy of the Starling EOS for light hydrocarbons (23 fluids) can be summarized as follows, [37]: densities are predicted with an average absolute deviation from experimental values of 1.38% for 971 datapoints. Enthalpy departures are predicted with an average absolute deviation from experimental values of 4.05 kJ/kg for 620 datapoints. Vapor pressure are predicted accurately, since the EOS is constrained to measures for 663 points, and are obtained by solving the Gibbs equation, or, which is the same, the equality of fugacities in the vapor and liquid phase. Substance specific EOS are even more precise, like the water and ammonia EOSs.

THERMOPROP contains two modules: TPSI, [30], and STANMIX, [8]. The mentioned MEOSs are implemented in TPSI and were extended to the calculation of nonconventional thermodynamic functions as shown in the following section. The TPSI database currently includes: ammonia, water, methane, propane, butane, isopentane, pentane, hexane, octane, R11, R12.

STANMIX uses the Peng Robinson cubic EOS modified by Stryjeck and Vera in order to achieve high accuracy for saturation pressure estimates of pure fluids, [40]. The correct prediction of saturation properties implies accuracy also in the dense gas region. The model is extended to multicomponent fluids, with the Wong-Sandler (WS) mixing rules [34]. This model can treat even highly nonideal mixtures, [41]. Thermodynamic functions for both pure fluids and mixtures were added to STANMIX and are shown in the following section as well. The STANMIX database contains data for 53 pure fluids and 66 binary interaction parameters and can easily be expanded as needed.

B Thermodynamic Functions for Modern Flow Solvers. ZFLOW uses an hybrid between the finite element (FE) and finite volume (FV) methods for the spatial discretization of systems of nonlinear conservation laws such as the Euler equations. The implemented numerical scheme is a high resolution upwind formulation for unstructured grids and general equations of state. The boundary treatment in the case of general gases is also implemented, [29,42,43].

We now briefly outline the nonconventional thermodynamic functions added to the THERMOPROP thermodynamic models, starting from the fluid dynamic model implemented in ZFLOW. This can be regarded as a model procedure for other flow solvers.

The Euler equations in conservative form can be written as

$$\frac{\partial \mathbf{u}}{\partial t}+\sum_{j=1}^{d}\frac{\partial \mathbf{f}_j(\mathbf{u})}{\partial x_j}=0, \tag{2.1}$$

where the conservative variable vector $\mathbf{u}$ and the vector components $\mathbf{f}_j(\mathbf{u})$ of the hyper-flux $\mathbf{F}(\mathbf{u})$ are given by

$$\mathbf{u}=\begin{bmatrix}\rho\\ \rho u^t\\ \rho w_i\end{bmatrix},\quad \mathbf{f}_j(\mathbf{u})=\begin{bmatrix}\rho w_j\\ (\rho u^t+P)w_j\\ \rho w_i w_j+P\delta_{ij}\end{bmatrix}, \tag{2.2}$$

ρ denotes density, u^t the stagnation (or total) energy (i.e., the sum of the internal and kinetic energy), P the pressure, w_j the components of the velocity vector $\mathbf{w}$, and δ_{ij} is the Kroenecker symbol · $A_j(\mathbf{u})$ is the Jacobian matrix of the Euler flux function, i.e.,

$$A_j(\mathbf{u})=\frac{\partial \mathbf{f}_j(\mathbf{u})}{\partial \mathbf{u}}. \tag{2.3}$$

The upwind numerical scheme used in ZFLOW requires the computation of the following partial derivatives of P:

$$\alpha=\left(\frac{\partial P}{\partial \rho}\right)_u,\quad \beta=\left(\frac{\partial P}{\partial u}\right)_\rho. \tag{2.4}$$

α and β must be evaluated from an EOS in the usual form $P=P(v,T)$, where v is the specific volume and T is the temperature. The sound speed c, defined as

$$c^2=\left(\frac{\partial P}{\partial \rho}\right)_s=-v^2\left(\frac{\partial P}{\partial v}\right)_s, \tag{2.5}$$

is also necessary.

When an implicit time integration scheme is employed, the entropy (s) is one of the prescribed quantities at an inflow boundary. The numerical procedure in this case requires the knowledge of two additional thermodynamic functions, namely

$$\chi=\left(\frac{\partial s}{\partial \rho}\right)_u,\quad \phi=\left(\frac{\partial s}{\partial u}\right)_\rho. \tag{2.6}$$

The Γ function defined as

$$\Gamma=1+\frac{\rho}{c}\left(\frac{\partial c}{\partial \rho}\right)_s=\frac{v^3}{2c^2}\left(\frac{\partial^2 P}{\partial v^2}\right)_s \tag{2.7}$$

is not necessary for the flow field simulation but it is useful to investigate nonclassical gas effects in the dense gas region.

All the mentioned thermodynamic functions can be expressed as algebraic functions of P, v, T starting from an EOS in the usual form $P=P(v,T)$ and an expression of the specific heat in the ideal gas state, $C_P^0(T)$, by using appropriate thermodynamic transformations. The resulting expressions are as follows:

$$c=\sqrt{-v^2\gamma\left(\frac{\partial P}{\partial v}\right)_T} \tag{2.8}$$

$$\beta=\frac{1}{C_v}\left(\frac{\partial P}{\partial T}\right)_v \tag{2.9}$$

$$\alpha=c^2-\beta P v^2 \tag{2.10}$$

$$\chi=-v^2\frac{P}{T} \tag{2.11}$$

$$\phi=\frac{1}{T} \tag{2.12}$$

$$\Gamma=\frac{v^3}{2c^2}\left\{\left(\frac{\partial^2 P}{\partial v^2}\right)_T-3\frac{T}{C_v}\left(\frac{\partial P}{\partial T}\right)_v\left(\frac{\partial^2 P}{\partial v\,\partial T}\right)_{v,T}+\left[\frac{T}{C_v}\left(\frac{\partial P}{\partial T}\right)_v\right]^2\left\{3\left(\frac{\partial^2 P}{\partial T^2}\right)_v+\frac{1}{T}\left(\frac{\partial P}{\partial T}\right)_v\left[1-\frac{T}{C_v}\left(\frac{\partial C_v}{\partial T}\right)_v\right]\right\}\right\}. \tag{2.13}$$

In Eqs. (2.8)–(2.13) the specific heat at constant pressure (C_P), at constant volume (C_v) and their ratio $\gamma=C_P/C_v$ can be calculated as

$$C_v^0(T)=C_p^0(T)-R \tag{2.14}$$

$$C_v=C_v^0(T)+T\int_\infty^v\left(\frac{\partial^2 P}{\partial T^2}\right)_v dv \tag{2.15}$$

$$C_P=C_v-\frac{T(\partial P/\partial T)_v^2}{(\partial P/\partial v)_T} \tag{2.16}$$

$$\gamma=1-\frac{T}{C_v}\frac{(\partial P/\partial T)_v^2}{(\partial P/\partial v)_T}. \tag{2.17}$$

To obtain Eqs. (2.8)–(2.13) from the definitions, thermodynamic relations and rules for partial derivatives transformation are used and details are reported in Appendix A. Expressions specific to the various thermodynamic models implemented in STANMIX and TPSI are reported in Appendix B.

Table 1 Comparison between CPU time needed for computing all thermodynamic properties, given 2 input variables, using either analytical expressions for calculating partial derivatives or a numerical discretization procedure, [45]. The *T*, *v* calculation is direct while calculations for other couples of input variables are iterative on *T*, *v*.

Input Variables	Thermodynamic Region	Input Variable 1	Input Variable 2	CPU Time[a] $\frac{f(x+h,y)-f(x,y)}{h}$	CPU Time[a] $\left(\frac{\partial f}{\partial x}\right)_y$
T, *v*	dense gas	$T=300°C$	$v=0.0109\ m^3/kg$	1710	137
(direct calculation)	perfect gas	$T=300°C$	$v=0.4116\ m^3/kg$	1595	138
T, *P*	dense gas	$T=300°C$	$P=22$ bar	1774	107
	perfect gas	$T=300°C$	$P=1$ bar	1740	106
h, *s*	dense gas	$h=905.10$ kJ/kg	$s=2.022$ kJ/kg K	22,822	21,307
	perfect gas	$h=977.16$ kJ/kg	$s=2.348$ kJ/kg K	4910	3200

[a]Time in milliseconds for 1000 cycles on an Intel Pentium II Processor, 400 MHz clock frequency, MS Windows NT 4.0 Operating System, Compaq Visual Fortran V6.5a Professional Edition, full optimization mode

The mentioned complex algebraic expressions can be more easily derived using software for symbolic calculations (see, e.g., Ref. [44]) and in some occasions it may prove an indispensable tool. The software, appropriately customized for thermodynamic functions treatment, can easily operate thermodynamic transformations, derivation, and integrations of algebraic expressions.

It is worthwhile noting that all the mentioned thermodynamic functions can be calculated from the EOS, $C_P^0(T)$, the partial derivatives

$$\left(\frac{\partial P}{\partial v}\right)_T, \quad \left(\frac{\partial P}{\partial T}\right)_v, \quad \left(\frac{\partial^2 P}{\partial v^2}\right)_T, \quad \left(\frac{\partial^2 P}{\partial T^2}\right)_v,$$

$$\left(\frac{\partial^2 P}{\partial T \partial v}\right)_{v,T}, \quad \left(\frac{\partial C_v}{\partial T}\right)_v,$$

and the integral

$$\int_\infty^v \left(\frac{\partial^2 P}{\partial T^2}\right)_v dv.$$

The importance of using analytical expression in CFD simulation must be stressed. The use of complex thermodynamic models in numerical flow solvers implies a considerable increase in CPU time if compared to the ideal gas approximation. All partial derivatives could also be computed numerically, using appropriate methods to get the needed accuracy. For example, in TPSI analytical expressions for partial derivatives for the water and ammonia EOSs were impractical to obtain due to the excessive complication of the EOS form, and an adaptive method, [45], was employed. It must be noted though that using analytical expressions greatly reduces the CPU time. Table 1 reports the comparison between the time for calculating all thermodynamic properties using partial derivatives computed with their analytical expression versus numerical discretization using the mentioned robust method. In the reported example, calculating partial derivatives with their analytical expression requires as few as 1/16 less computing time.

3 Sound Speed and the Fundamental Derivative of Gas Dynamics for Several Classes of Fluids

As it is shown in the preceding section, the convective sound speed can be computed from its definition using an EOS in the usual form $P=P(v,T)$. The accuracy of the computed values directly affects the correctness of the computed flow field and, because of its dependence on the derivative of the main thermodynamic variables, relies on the capability of the EOS of correctly describing the combination of volumetric and thermal molecular interaction. This requires a complex EOS, especially if part of the flow field is in thermodynamic states close to the critical region, as it is the case when investigating dense or nonclassical fluid dynamics effects.

Furthermore, the parameter Γ, depending on second partial derivatives, shows a more accentuate dependance on the algebraic form of the EOS and its estimation shows considerable differences as it will be illustrated in Section 3B.

A Sound Speed Estimates. In order to assess the accuracy of the thermodynamic models implemented in THERMOPROP when computing the sound speed, calculations along isotherms and isobars in widely different thermodynamic regions are compared with either experimental measurements or reference data for selected substances. It must be noted that sound speed data for comparison pertaining to fluids whose molecule is sufficiently complex to suppose nonclassical fluid dynamic behavior are not available. Nevertheless, the accuracy of the thermodynamic models implemented in THERMOPROP can be qualitatively extrapolated from the results described in the following.

As a first classical test case, TPSI and STANMIX sound speed computed values for water are compared with reference data made available by the National Institute of Standards and Technologies (NIST), [46]. Figure 1 shows that the accuracy of the modified Keenan and Keyes model implemented in TPSI, [30,35], is very high even in the liquid region and in the proximity of the critical point. Results for the cubic EOS implemented in STANMIX are shown in Fig. 2: As expected, the PRSV EOS is not accurate in the liquid region (calculated points are omitted), and close to the critical point.

Hexane is employed as working fluid in geothermal organic Rankine cycles: sound speed results obtained with the Starling EOS implemented in TPSI for values of pressure and temperature in the vapor phase (Fig. 3) are very accurate if compared to NIST reference data.

In recent years highly accurate speed of sound measurements have become available, thanks also to a recently developed experimental method, [47]. Experimental data for refrigerant R125 found in the literature are compared to STANMIX sound speed calculations in Fig. 4. The available experimental data are in the range 0.5/5 bar and $-13/86°C$, and therefore the fluid is not far from the ideal gas state. As it can be noted, deviations in this case are very small.

B The Fundamental Derivative Γ for Several Fluids and Mixtures. Classes of fluids that are used in technical applications include organic and inorganic substances. Table 2 reports several classes of fluids and examples of their technical use. All the mentioned fluids can be used in applications that require investigation of dense gas or nonclassical gas effects. Siloxanes were recently proposed and adopted as working fluids for ORC turbines. Together with favorable thermodynamic characteristics with respect to cycle and turbine design, they are thermally stable, atoxic, and scarcely flammable. Moreover, because of their molecular complexity, they may exhibit nonclassical behavior in the dense gas region.

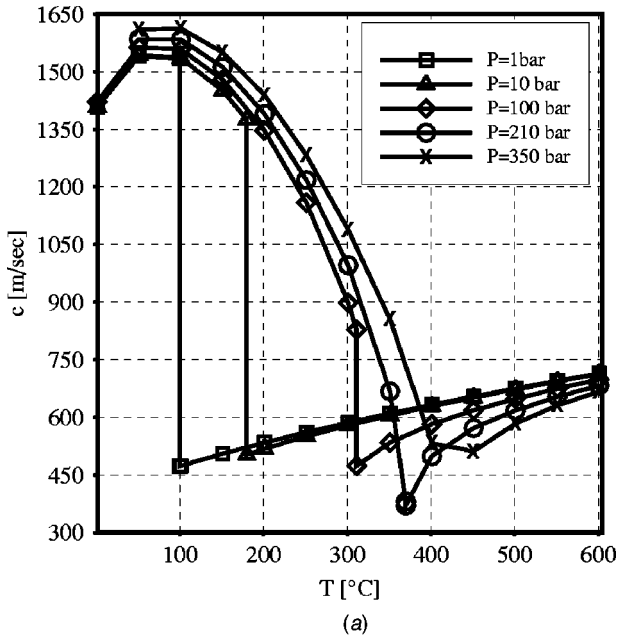

(a)

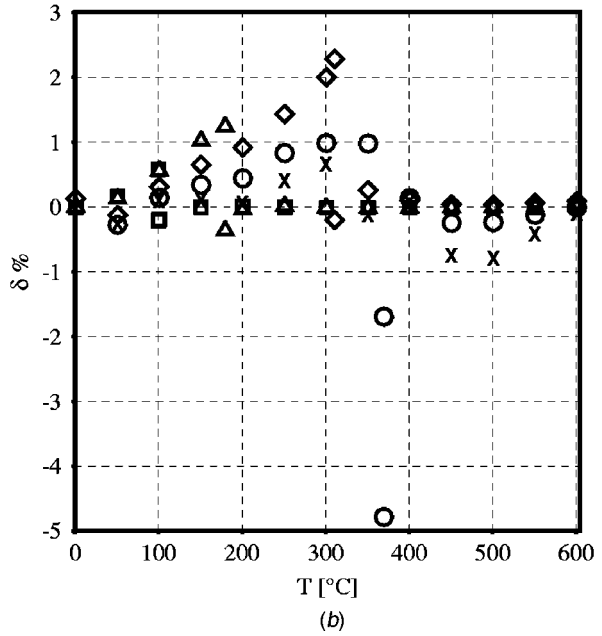

(b)

Fig. 1 Water TPSI sound speed estimations comparison with NIST highly accurate data, [62]. δ%: deviation from NIST data; c: TPSI sound speed estimations. Water critical point: T_c = 374.15°C; P_c = 221 bar.

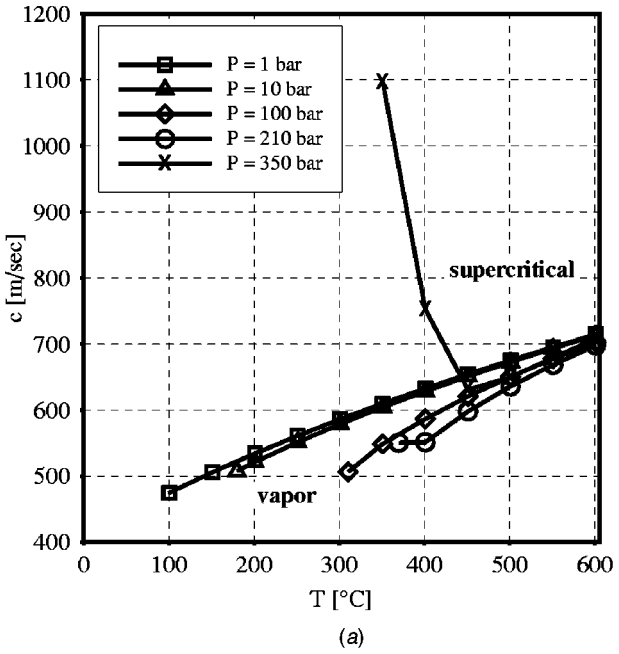

(a)

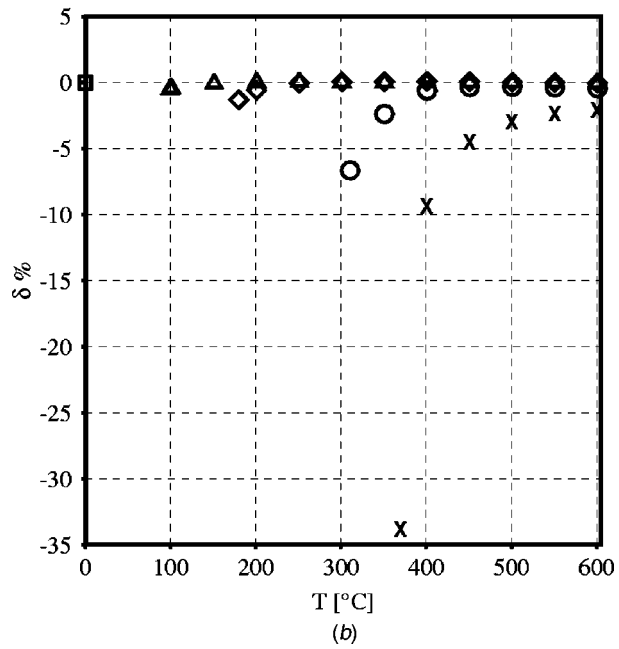

(b)

Fig. 2 Water vapor STANMIX sound speed estimations comparisons with reference data, [62]. δ%: deviation from NIST data; c: sound speed values calculated by STANMIX. Water critical point: T_c = 374.14°C; P_c = 220.8975 bar.

1 Comparison With Published Literature. In order to assess differences and further validate Γ calculated with the thermodynamic models implemented in THERMOPROP, values along the critical isotherms for several common fluids are compared with curves reported by other investigators, [10,48].

As it can be noted in Figs. 5, 6, and 7 values can differ substantially for relative densities greater than 0.5, and this is expected because differences between thermodynamic models increase in the critical region. Values calculated with substance-specific EOS for water and n-Octane, like the ones implemented in TPSI, are more accurate because those EOS are fitted to experimental data even in the near-critical region while the Martin-Hou EOS, being more general, cannot be as accurate.

Figures 6 and 7 show, moreover, that the cubic EOS of the STANMIX model, even if it predicts a quite different curve shape, nevertheless gives values that are intermediate between the Martin-Hou EOS and the substance-specific EOS, except for the region close to the critical point where it is known that CEOS's fail to the predict the correct behavior. This anyhow implies that this simpler EOS can be useful for preliminary investigation of fluids that could exhibit nonclassical behavior, with the advantage of needing less experimental input data for the model.

In Fig. 8, a more comprehensive chart extends the work reported in Ref. [49] with some of the fluids of THERMOPROP: It can be seen that in general THERMOPROP Γ values are more conservative with respect to predicting nonclassical behavior.

In order to show the thermodynamic region where the turbine expansion of an ORC is located, in Fig. 9 the transformation is

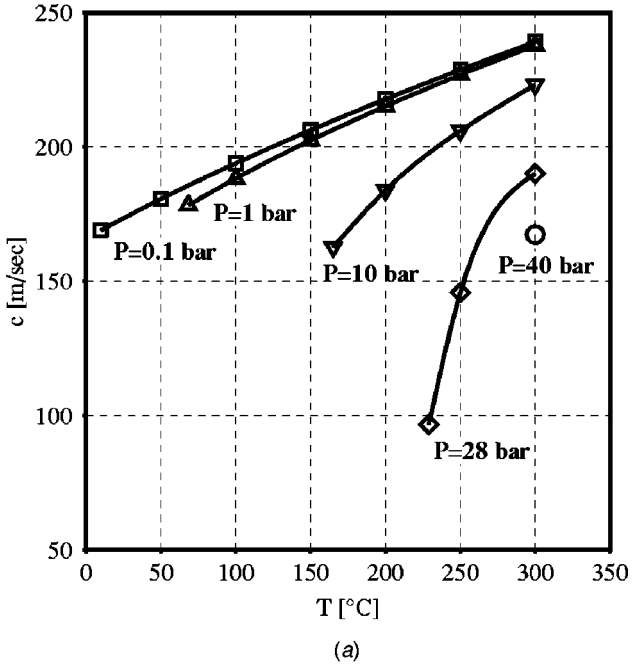

(*a*)

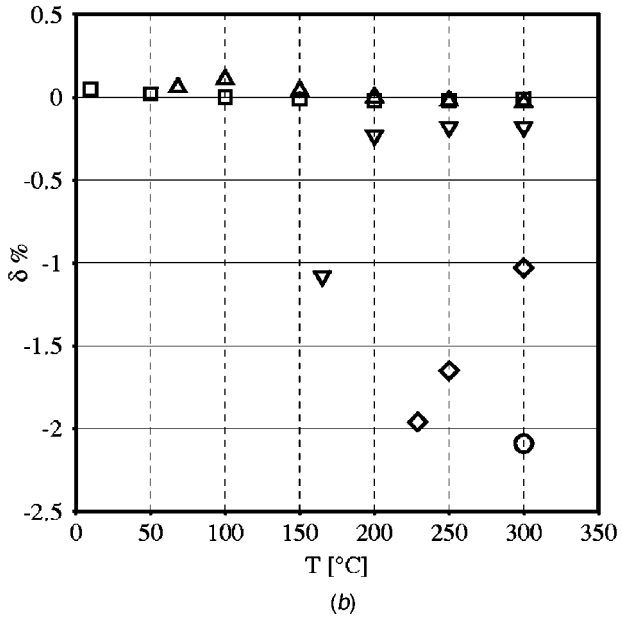

(*b*)

Fig. 3 Hexane TPSI sound speed estimations in the vapor phase versus NIST reference data, [63]. *δ*%: deviation from NIST data; *c*: TPSI sound speed estimations. Hexane critical point: T_c=232.98°C; P_c=29.27 bar.

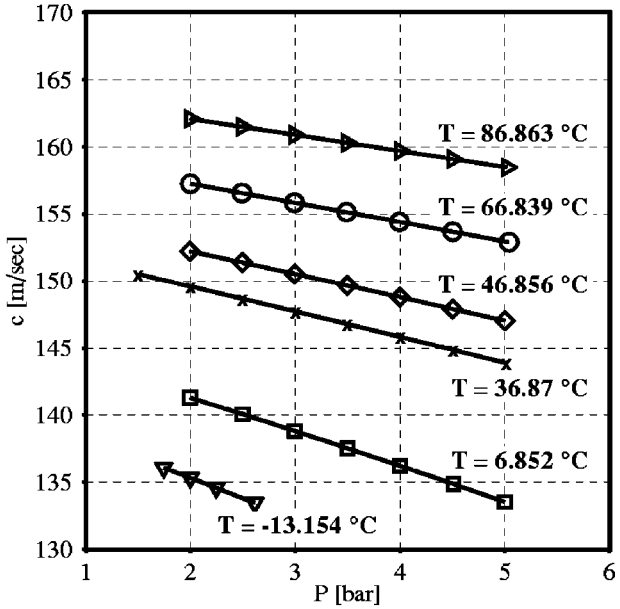

(*a*)

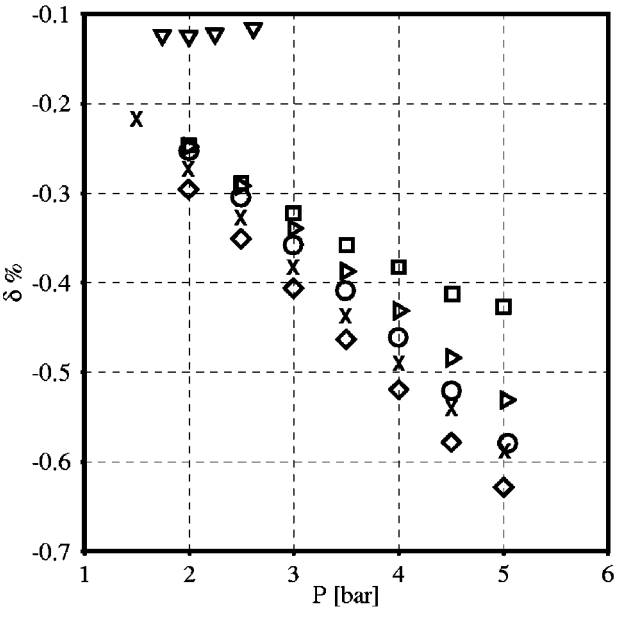

(*b*)

Fig. 4 STANMIX sound speed estimations for R125: comparison with experimental data in Ref. [64]. *δ*%: deviation from experimental data; *c*: sound speed values calculated by STANMIX. R125 critical point: T_c=66.25°C; P_c=36.31 bar.

qualitatively represented. In the region where Γ is small even if still positive, nonclassical gasdynamics effects may occur (see, e.g., Ref. [23]).

2 Siloxanes. Γ values for siloxanes calculated with STANMIX are presented in Fig. 10. In Tables 3 and 4 and in Figs. 10, 11, 12 the common nomenclature for fluids belonging to the siloxane class is the original introduced by Wilcock [50]. Input data for the models are obtained from Dow Corning and thermodynamic properties validation is documented in previous works, [8,51].

In Fig. 10(*a*) are reported Γ curves along the critical isotherms for several linear siloxanes: Note that the values at the critical point are almost the same for all molecules containing the D

Table 2 Classes of fluids for technical applications that can involve their use in the dense gas region

	Fluid	Applications
organic	hydrocarbons	chemical and petrochemical processes, geothermal ORC
	fluorocarbons	chemical processes, refrigeration, geothermal ORC
	siloxanes	high temperature ORC
inorganic	ammonia	refrigeration, Kalina power cycle
	light gases	cryogenic processes, air distillation

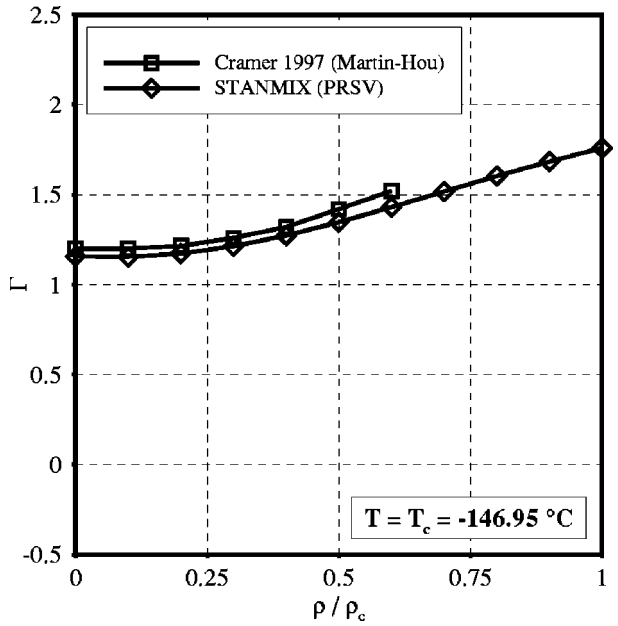

Fig. 5 Comparison between nitrogen Γ along the critical isotherm calculated by StanMix (PRSV EOS) and literature values (Martin-Hou EOS), [10]

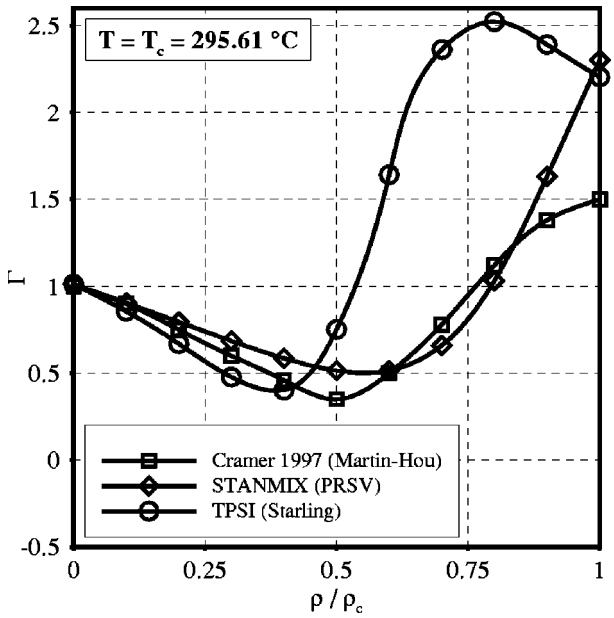

Fig. 7 Comparison between n-Octane Γ along the critical isotherm calculated by StanMix (PRSV EOS), TPSI (Starling), and literature values (Martin-Hou EOS), [10]

groups, $(CH_3)_2SiO$, and it is different for MM which is the simplest molecule and contains only M groups, $(CH_3)_3SiO_{1/2}$. In Fig. 10(*b*) estimates for cyclic siloxanes can be compared to those of linear siloxanes previously outlined: cyclic molecules of comparable molecular weight are slightly less complex, therefore Γ values are higher.

Figure 11 shows Γ values along several isotherms for MD_4M, calculated by StanMix: For subcritical temperature values and for relative specific densities between 1.5 and 2 a negative Γ region is outlined. By observing the shape of Γ curves along isotherms, it can be deduced from Fig. 10 that negative subcritical Γ regions are also found for linear siloxanes lighter than MD_4M, and for cyclic siloxanes. Linear and cyclic siloxanes are therefore very likely Bethe-Zel'dovic-Thompson (BZT) fluids, according to Cramer's definition, [23], of BZT fluids as those having a negative Γ region.

3 Mixtures

(a) Siloxanes. Figure 12 shows a comparison between pure linear siloxanes and equimolar mixtures of the same components. In order to display the calculated Γ values as a function of the

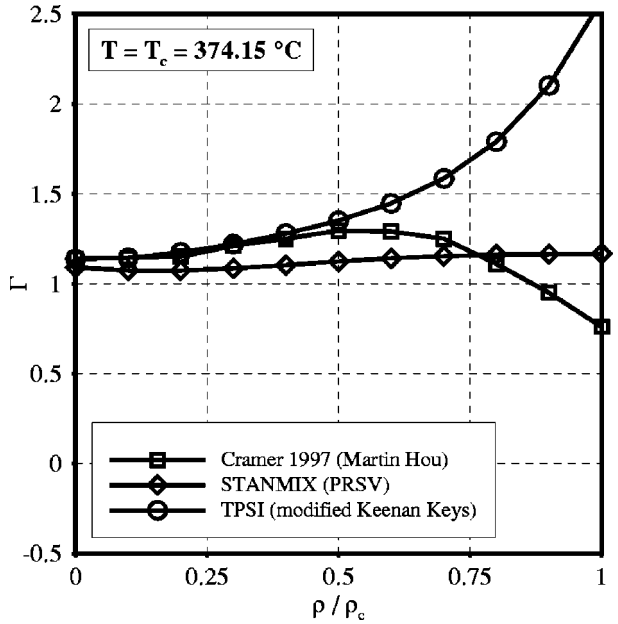

Fig. 6 Comparison between water Γ along the critical isotherm calculated by StanMix (PRSV EOS), TPSI (modified Keenan Keys), and literature values (Martin-Hou EOS), [10]

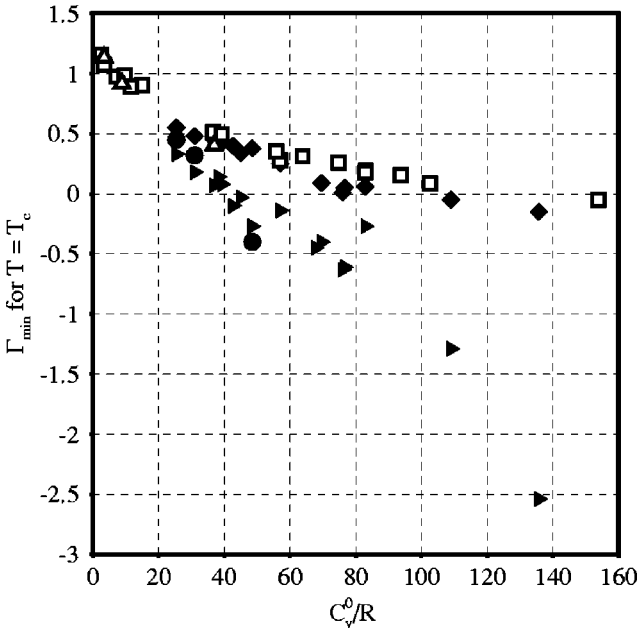

Fig. 8 An overview of minimum Γ along the critical isotherm predicted by StanMix, TPSI and several other equations of state as reported in the literature, [49]. □: StanMix (PRSV EOS), for several fluids; △: TPSI (MEOS), for several fluids; ♦: Martin-Hou, for several fluids; ►: Hirschfelder et al., for several fluids; ●: Benedict-Web-Rubin, for several fluids.

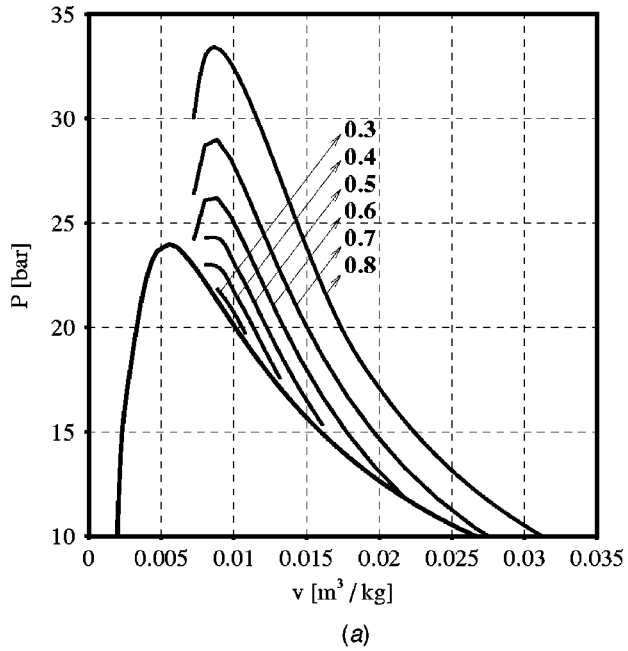

(*a*)

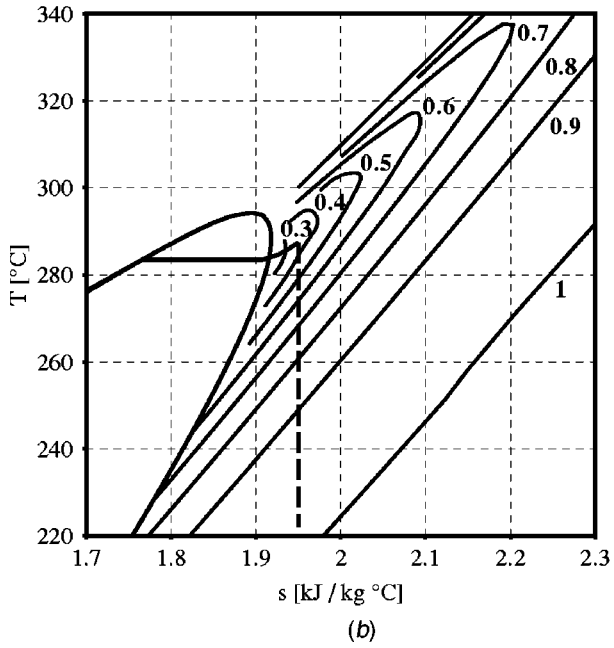

(*b*)

Fig. 9 Iso-Γ curves in the *P*−*v* (*a*) and *T*−*s* (*b*) thermodynamic plane for n-Octane (TPSI). Part of a typical ORC thermodynamic cycle is also represented in (*b*). The turbine expansion transformation for an ORC is qualitatively outlined (dashed line). As it can be noted part of the transformation takes place in the Γ<1 region. All curves are a graphical output from zFLOW.

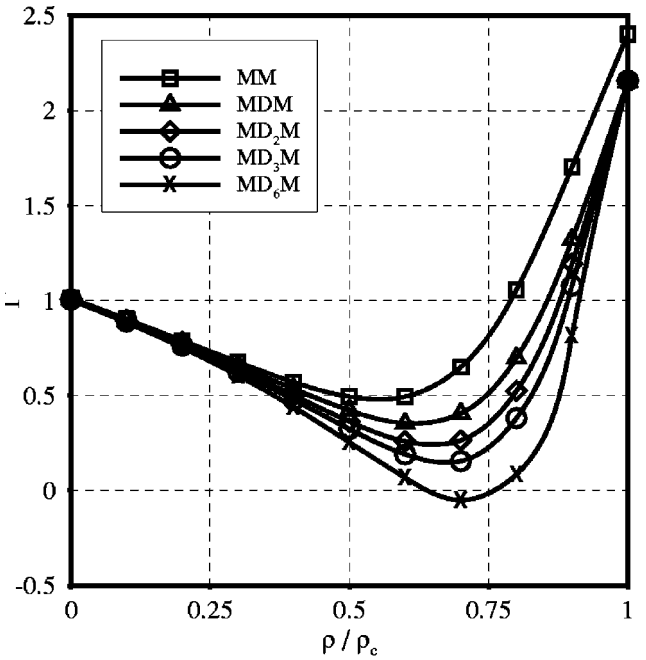

(*a*)

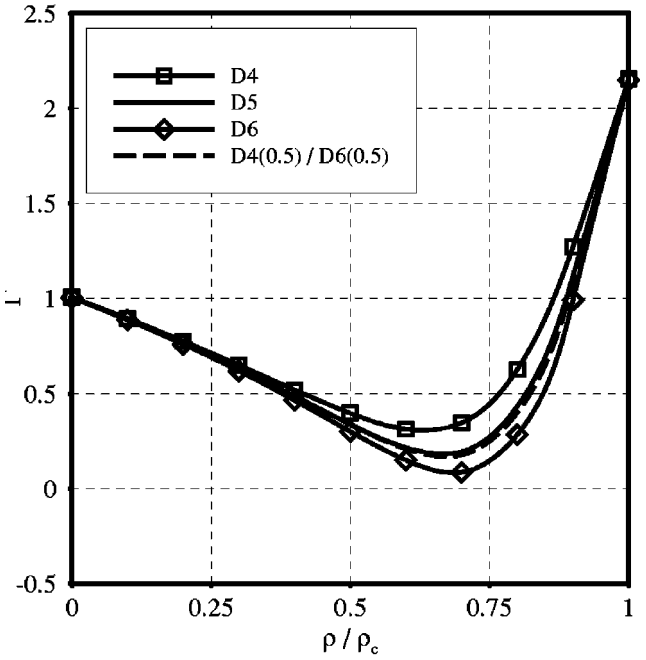

(*b*)

Fig. 10 Γ along the critical isotherm calculated by STANMIX (PRSV EOS) for several linear (*a*) and cyclic (*b*) siloxanes. A comparison between pure fluids and a mixture of the same fluids is also shown (dashed line in (*b*)).

relative density, so that they can be compared with pure fluid calculations and they are consistent with the usual representation of such results, the mixture critical density must also be computed. The direct calculation of the critical point for mixture is not implemented in the STANMIX code yet, therefore at the moment the critical parameters are evaluated graphically from the saturation curves in the $P-v$ plane and extrapolated. This reflects in an uncertainty in the mixture critical volume and therefore in the ρ/ρ_c coordinate. Siloxanes mixtures are almost ideal and very similar to light hydrocarbons with regard to molecular structure, therefore it is believed that their thermodynamic behavior is almost linear with molar composition: in this case, for example, an equimolar mixture of MD_nM and $MD_{n+2}M$ is almost equivalent to $MD_{n+1}M$. This is very well verified for the comparison of $MDM(0.5)/MD_3M(0.5)$ with MD_2M. In the case of the comparison of $MM(0.5)/MD_2M(0.5)$ with MDM, a certain discrepancy can be noted, and it is believed to be due to the slight difference between the MM and the MD_nM molecule structures and to the

Table 3 Basic thermodynamic parameters for lighter linear siloxanes, [61]

Name	Chemical Formula	T_c (°C)	P_c (bar)	MW
MM	$C_6H_{18}OSi_2$	245.60	19.3936	162.379
MDM	$C_8H_{24}O_2Si_3$	291.25	14.3983	236.530
MD_2M	$C_{10}H_{30}O_3Si_4$	326.25	11.7940	310.690
MD_3M	$C_{12}H_{36}O_4Si_5$	355.25	9.96024	384.843
MD_4M	$C_{14}H_{42}O_5Si_6$	380.00	8.77474	459.000

Table 4 Basic thermodynamic parameters for lighter cyclic siloxanes [61]

Name	Chemical Formula	T_c (°C)	P_c (bar)	MW
D_3	$((CH_3)_2SiO)_3$	281.05	16.63	222.464
D_4	$((CH_3)_2SiO)_4$	313.35	13.32	296.618
D_5	$((CH_3)_2SiO)_5$	346.00	11.60	370.773

uncertainty in the critical volume estimation for the mixture. The linear behavior is also very well outlined in Fig. 10(*b*) for cyclic siloxanes: The Γ curve for the equimolar mixture of D_4 and D_6 is almost identical to the curve for D_5.

(b) Other mixtures of technological interest. As a last example of the capability of the mixture model implemented in STANMIX, Fig. 13(*a*) shows Γ curves for air: In this case air is treated as a binary mixture of nitrogen(0.79)/oxygen (0.21) and curves for the pure components are also displayed.

One of the main characteristics of the mixture model coded in STANMIX is that it can treat both quasi-ideal mixtures and highly nonideal mixtures. Figure 13(*b*) shows the calculation of Γ along the critical isotherm for the aqueous 2-propanol mixture.

Mixtures of polar components were recently proposed as working fluids for power cycles (e.g., Kalina cycle [52–57], SMR cycle [58]) and for refrigeration cycles (see, e.g., Ref. [59]).

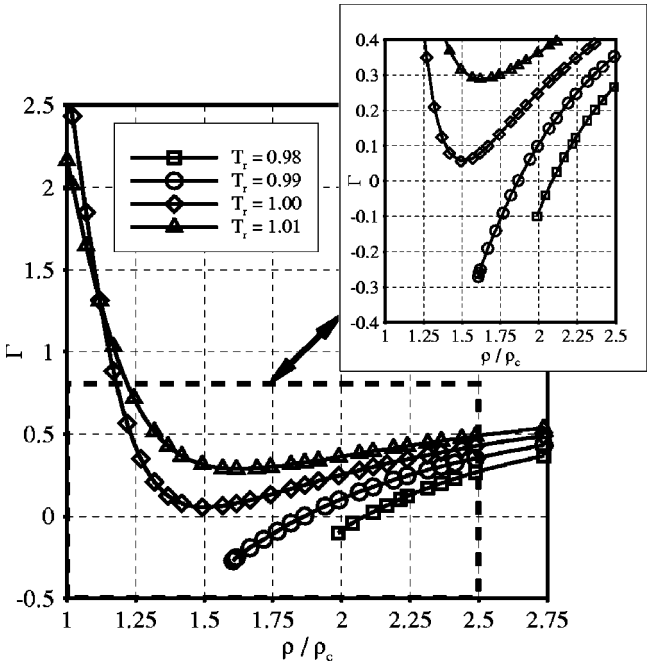

Fig. 11 MD_4M Γ along several isotherms calculated by STANMIX (PRSV EOS)

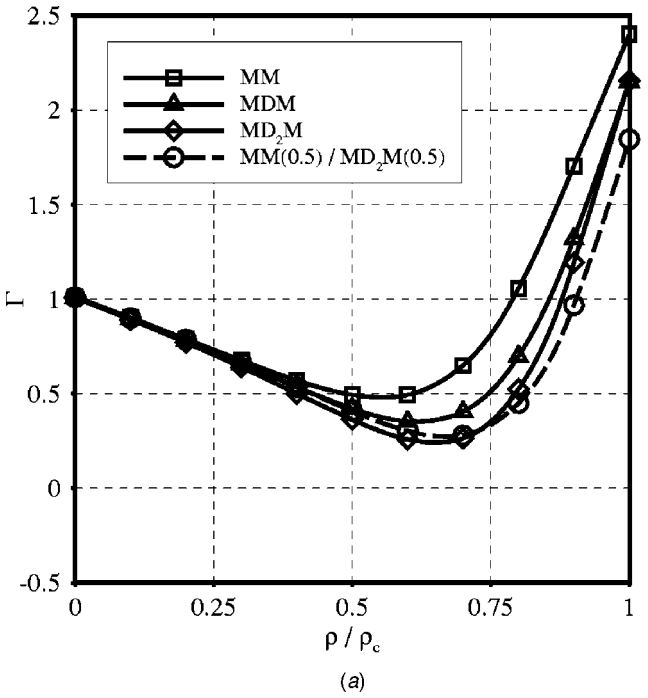

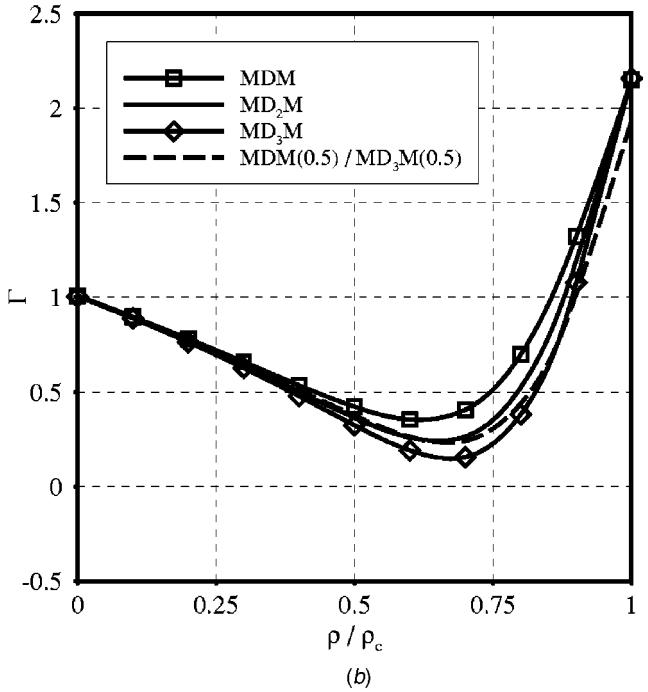

Fig. 12 Γ along the critical isotherm calculated by STANMIX (PRSV EOS) for linear siloxanes. Comparisons between pure fluids and mixtures of the same fluids.

4 Concluding Remarks

Modern numerical schemes for fluid dynamics simulations need complex thermodynamic models if dense or nonclassical gas effects are investigated. Previous work documented the use of Van der Waals or Martin Hou equations of state or other relatively simple models. In this work, the procedures for incorporating more complex EOS and EOS for mixtures in fluid dynamics solvers are presented. In order to speed up calculations, algebraic expressions for nonconventional thermodynamic properties must be

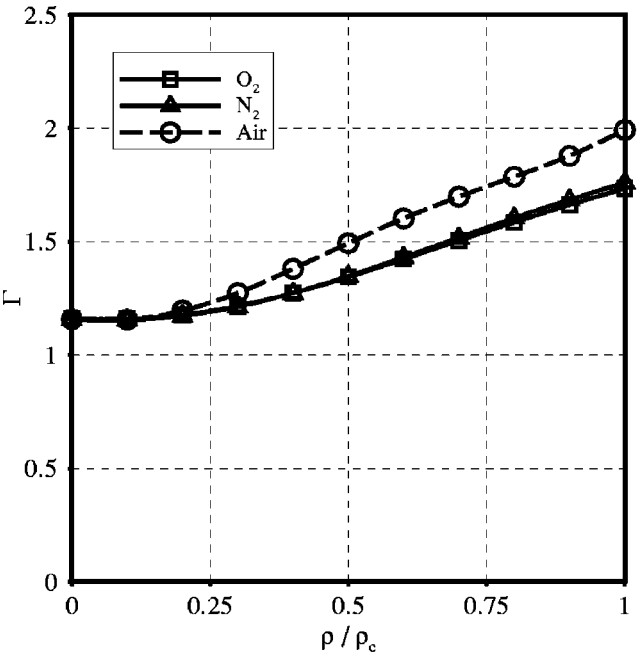

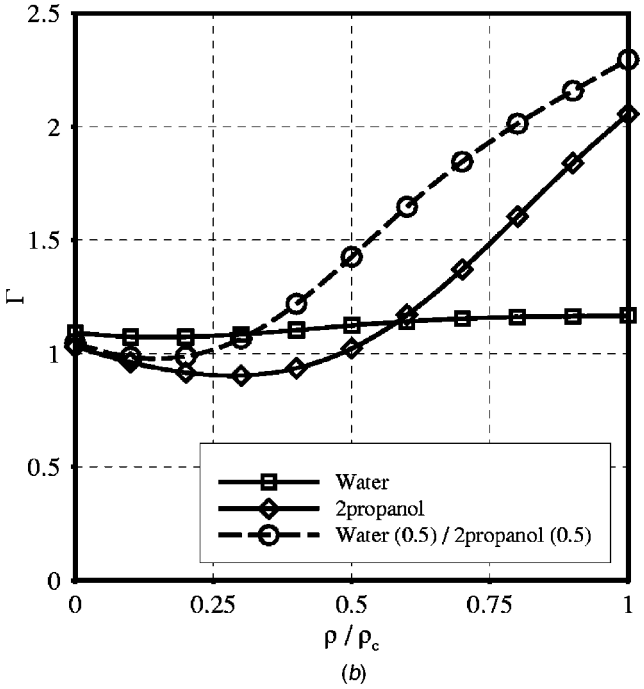

Fig. 13 Γ along the critical isotherm calculated by StanMix (PRSV EOS) for air (*a*) and an equimolar aqueous-2propanol mixture (*b*), a highly nonideal mixture. Air is approximated with a binary mixture of 0.79 nitrogen and 0.21 oxygen (mole fractions).

added to common thermodynamic properties programs. The accuracy of the implemented thermodynamic models can be deduced also from the comparison of sound speed estimates with experimental or reference data. The extension of existing thermodynamic models enable us to treat a wide variety of fluids with the PRSV EOS and a smaller but still considerable set of fluids with more complex EOS. The use of state-of-the art mixing rules extends the cubic equation of state model to ideal and highly nonideal mixtures. The evaluation of the fundamental derivative of gasdynamics Γ for Siloxanes is presented for the first time. Siloxanes form a class of substances of technological interest because they can be used as working fluids in organic Rankine cycles. Some of the linear and cyclic siloxanes and their mixtures exhibit negative Γ regions that could be exploited in the design of more efficient turbines. Results of fluid dynamic simulations of mono and two-dimensional channel configurations will be presented in upcoming publications. An extension of the code to the solution of viscous flows and to multiphase fluids is also planned.

Acknowledgments

The authors are very grateful to their friend and colleague S. Rebay for his advice. We also gratefully recognize Prof. W. C. Reynolds, Mechanical Engineering Department, Stanford University, for his guidance in the initial phase of this project and the permit to extend his software TPSI.

Appendix A

Nonconventional Thermodynamic Functions for Computational Fluid Dynamics From Equations of State

1 Partial Derivatives of Pressure: α and β. The definition of α and β is

$$\alpha=\left(\frac{\partial P}{\partial \rho}\right)_u=-v^2\left(\frac{\partial P}{\partial v}\right)_u, \tag{A1}$$

$$\beta=\left(\frac{\partial P}{\partial u}\right)_\rho=\left(\frac{\partial P}{\partial u}\right)_v. \tag{A2}$$

By using the chain rule expansion, β can be written as

$$\beta=\frac{(\partial P/\partial T)_v}{(\partial u/\partial T)_v}. \tag{A3}$$

Therefore it can be evaluated from a volumetric EOS and the specific heat at constant volume as

$$\beta=\frac{1}{C_v}\left(\frac{\partial P}{\partial T}\right)_v. \tag{A4}$$

The relation between α, c, and β can be obtained as shown in the following. Using the chain rule expansion yields

$$\left(\frac{\partial P}{\partial v}\right)_u\left(\frac{\partial v}{\partial u}\right)_P\left(\frac{\partial u}{\partial P}\right)_v=-1,$$
$$\left(\frac{\partial P}{\partial v}\right)_u=-\left(\frac{\partial u}{\partial v}\right)_P\left(\frac{\partial P}{\partial u}\right)_v=-\left(\frac{\partial u}{\partial v}\right)_P\beta. \tag{A5}$$

Therefore α can be written as

$$\alpha=v^2\beta\left(\frac{\partial u}{\partial v}\right)_P. \tag{A6}$$

The latter partial derivative can be written as

$$\left(\frac{\partial u}{\partial v}\right)_P=\frac{(\partial u/\partial T)_P}{(\partial v/\partial T)_P}, \tag{A7}$$

and from usual thermodynamic derivation,

$$\left(\frac{\partial u}{\partial T}\right)_P=C_v+\left[T\left(\frac{\partial P}{\partial T}\right)_v-P\right]\left(\frac{\partial v}{\partial T}\right)_P. \tag{A8}$$

By substituting Eq. (*A*7) in Eq. (*A*6) and simplifying, the expression for α becomes

$$\alpha=v^2\beta\left[\frac{C_v}{(\partial v/\partial T)_P}+T\left(\frac{\partial P}{\partial T}\right)_v-P\right]. \tag{A9}$$

Using the chain rule yields

$$\left(\frac{\partial v}{\partial T}\right)_P = -\left(\frac{\partial P}{\partial T}\right)_v \left(\frac{\partial v}{\partial P}\right)_T. \tag{A10}$$

By recalling that the relation between C_P and C_v is

$$C_P = C_v - \frac{T(\partial P/\partial T)_v^2}{(\partial P/\partial v)_T}, \tag{A11}$$

the following expression is obtained:

$$\left(\frac{\partial v}{\partial P}\right)_T = \frac{C_v - C_P}{T(\partial P/\partial T)_v^2}. \tag{A12}$$

Substituting Eq. (*A*12) in Eq. (*A*10) yields

$$\left(\frac{\partial v}{\partial T}\right)_P = \frac{C_P - C_v}{T(\partial P/\partial T)_v}. \tag{A13}$$

From Eq. (2.8), the specific volume can be written as

$$v^2 = -\frac{c^2}{\gamma(\partial P/\partial v)_T}, \tag{A14}$$

therefore substituting Eq. (*A*13), Eq. (*A*4), and Eq. (*A*14) in Eq. (*A*9) yields

$$\alpha = -\frac{c^2}{\gamma(\partial P/\partial v)_T}\frac{1}{C_v}\left(\frac{\partial P}{\partial T}\right)_v \left[\frac{C_v T(\partial P/\partial T)_v}{C_P - C_v} + T\left(\frac{\partial P}{\partial T}\right)_v\right] - \beta P v^2. \tag{A15}$$

By carrying out straightforward simplifications and by recalling that

$$C_P - C_v = -T\left(\frac{\partial P}{\partial T}\right)_v^2 \left(\frac{\partial v}{\partial P}\right)_T, \tag{A16}$$

the following expression is finally obtained:

$$\alpha = c^2 - \beta P v^2. \tag{A17}$$

2 Partial Derivatives of Entropy: χ *and* ϕ. The definition of χ and ϕ is

$$\chi = \left(\frac{\partial s}{\partial \rho}\right)_u = -v^2\left(\frac{\partial s}{\partial v}\right)_u \tag{A18}$$

$$\phi = \left(\frac{\partial s}{\partial u}\right)_\rho = \left(\frac{\partial s}{\partial u}\right)_v. \tag{A19}$$

The differential of entropy can be expressed as

$$ds = \frac{1}{T}du - \frac{P}{T}dv.$$

Therefore,

$$\left(\frac{\partial s}{\partial v}\right)_u = \frac{P}{T},$$

$$\left(\frac{\partial s}{\partial u}\right)_v = \frac{1}{T},$$

$$\chi = -v^2\frac{P}{T}, \tag{A20}$$

$$\phi = \frac{1}{T}. \tag{A21}$$

3 The Fundamental Derivative of Gas Dynamics: Γ. The expression of Γ in terms which allow its calculation from a volumetric EOS is reported, for instance, in Refs. [23], [60]. We hereby report its derivation.

The parameter Γ is defined as

$$\Gamma = 1 + \frac{\rho}{c}\left(\frac{\partial c}{\partial \rho}\right)_s = \frac{v^3}{2c^2}\left(\frac{\partial^2 P}{\partial v^2}\right)_s. \tag{A22}$$

The composite derivative rule applied to $(\partial^2 P/\partial v^2)_s$ can explicitly be written as

$$\left[\frac{\partial}{\partial v}\left(\frac{\partial P}{\partial v}\right)_s\right]_s = \left(\frac{\partial^2 P}{\partial v^2}\right)_s = \left[\frac{\partial}{\partial v}\left(\frac{\partial P}{\partial v}\right)_s\right]_T + \left[\frac{\partial}{\partial T}\left(\frac{\partial P}{\partial v}\right)_s\right]_v \left(\frac{\partial T}{\partial v}\right)_s.$$

Substituting for $(\partial^2 P/\partial v^2)_s$ the following expression is obtained:

$$\begin{aligned}\left(\frac{\partial^2 P}{\partial v^2}\right)_s &= \frac{\partial}{\partial v}\left[\left(\frac{\partial P}{\partial T}\right)_v\left(\frac{\partial T}{\partial v}\right)_s + \left(\frac{\partial P}{\partial v}\right)_T\right]_T \\ &\quad + \left\{\frac{\partial}{\partial T}\left[\left(\frac{\partial P}{\partial T}\right)_v\left(\frac{\partial T}{\partial v}\right)_s + \left(\frac{\partial P}{\partial v}\right)_T\right]_v\right\}\left(\frac{\partial T}{\partial v}\right)_s \\ &= \left(\frac{\partial^2 P}{\partial v\,\partial T}\right)_{v,T}\left(\frac{\partial T}{\partial v}\right)_s + \frac{\partial}{\partial v}\left[\left(\frac{\partial T}{\partial v}\right)_s\right]_T\left(\frac{\partial P}{\partial T}\right)_v + \left(\frac{\partial^2 P}{\partial v^2}\right)_T \\ &\quad + \left(\frac{\partial^2 P}{\partial T^2}\right)_v\left(\frac{\partial T}{\partial v}\right)_s^2 + \left(\frac{\partial^2 P}{\partial v\,\partial T}\right)_{v,T}\left(\frac{\partial T}{\partial v}\right)_s \\ &\quad + \left(\frac{\partial P}{\partial T}\right)_v\frac{\partial}{\partial T}\left[\left(\frac{\partial T}{\partial v}\right)_s\right]_v\left(\frac{\partial T}{\partial v}\right)_s \\ &= 2\left(\frac{\partial^2 P}{\partial v\,\partial T}\right)_{v,T}\left(\frac{\partial T}{\partial v}\right)_s + \frac{\partial}{\partial v}\left[\left(\frac{\partial T}{\partial v}\right)_s\right]_T\left(\frac{\partial P}{\partial T}\right)_v + \left(\frac{\partial^2 P}{\partial v^2}\right)_T \\ &\quad + \left(\frac{\partial^2 P}{\partial T^2}\right)_v\left(\frac{\partial T}{\partial v}\right)_s^2 + \left(\frac{\partial P}{\partial T}\right)_v\frac{\partial}{\partial T}\left[\left(\frac{\partial T}{\partial v}\right)_s\right]_v\left(\frac{\partial T}{\partial v}\right)_s. \end{aligned} \tag{A23}$$

From usual thermodynamic derivation,

$$\left(\frac{\partial T}{\partial v}\right)_s = -\frac{T}{C_v}\left(\frac{\partial P}{\partial T}\right)_v. \tag{A24}$$

Equation (*A*24) can be substituted in Eq. (*A*23) and the following expression is obtained:

$$\begin{aligned}\left(\frac{\partial^2 P}{\partial v^2}\right)_s &= -2\frac{T}{C_v}\left(\frac{\partial^2 P}{\partial v\,\partial T}\right)_{v,T}\left(\frac{\partial P}{\partial T}\right)_v + \frac{\partial}{\partial v}\left[-\frac{T}{C_v}\left(\frac{\partial P}{\partial T}\right)_v\right]_T\left(\frac{\partial P}{\partial T}\right)_v \\ &\quad + \left(\frac{\partial^2 P}{\partial v^2}\right)_T + \left(\frac{\partial^2 P}{\partial T^2}\right)_v\left[-\frac{T}{C_v}\left(\frac{\partial P}{\partial T}\right)_v\right]^2 \\ &\quad + \left(-\frac{T}{C_v}\right)\left(\frac{\partial P}{\partial T}\right)_v^2\frac{\partial}{\partial T}\left[-\frac{T}{C_v}\left(\frac{\partial P}{\partial T}\right)_v\right]_v. \end{aligned}$$

By developing the partial derivatives and appropriately collecting terms, $(\partial^2 P/\partial v^2)_s$ can be written as

$$\begin{aligned}\left(\frac{\partial^2 P}{\partial v^2}\right)_s &= \left(\frac{\partial^2 P}{\partial v^2}\right)_T - 3\frac{T}{C_v}\left(\frac{\partial P}{\partial T}\right)_v\left(\frac{\partial^2 P}{\partial v\,\partial T}\right)_{v,T} + 3\frac{T}{C_v^2}\left(\frac{\partial P}{\partial T}\right)_v^2\left(\frac{\partial C_v}{\partial v}\right)_T \\ &\quad + \frac{T}{C_v^2}\left(\frac{\partial P}{\partial T}\right)_v^3\left[1 - \frac{T}{C_v}\left(\frac{\partial C_v}{\partial T}\right)_v\right]. \end{aligned}$$

Furthermore, the partial derivative of the specific heat with respect to the specific volume at constant temperature can be expressed as

$$\left(\frac{\partial C_v}{\partial v}\right)_T=\frac{\partial}{\partial v}\left[\left(\frac{\partial u}{\partial T}\right)_v\right]_T=\frac{\partial}{\partial T}\left[\left(\frac{\partial u}{\partial v}\right)_T\right]_v$$
$$=\frac{\partial}{\partial T}\left[T\left(\frac{\partial P}{\partial T}\right)_v-P\right]_v=T\left(\frac{\partial^2 P}{\partial T^2}\right)_v.$$

Therefore the final expression for $(\partial^2 P/\partial v^2)_s$ is

$$\left(\frac{\partial^2 P}{\partial v^2}\right)_s=\left(\frac{\partial^2 P}{\partial v^2}\right)_T-3\frac{T}{C_v}\left(\frac{\partial P}{\partial T}\right)_v\left(\frac{\partial^2 P}{\partial v\,\partial T}\right)_{v,T}+3\frac{T^2}{C_v^2}\left(\frac{\partial P}{\partial T}\right)_v^2\left(\frac{\partial^2 P}{\partial T^2}\right)_v$$
$$+\frac{T}{C_v^2}\left(\frac{\partial P}{\partial T}\right)_v^3\left[1-\frac{T}{C_v}\left(\frac{\partial C_v}{\partial T}\right)_v\right]$$
$$=\left(\frac{\partial^2 P}{\partial v^2}\right)_T-3\frac{T}{C_v}\left(\frac{\partial P}{\partial T}\right)_v\left(\frac{\partial^2 P}{\partial v\,\partial T}\right)_{v,T}+\left[\frac{T}{C_v}\left(\frac{\partial P}{\partial T}\right)_v\right]^2$$
$$\times\left\{3\left(\frac{\partial^2 P}{\partial T^2}\right)_v+\frac{1}{T}\left(\frac{\partial P}{\partial T}\right)_v\left[1-\frac{T}{C_v}\left(\frac{\partial C_v}{\partial T}\right)_v\right]\right\}. \quad (A25)$$

This expression compares with the one reported in Ref. [60].

By recalling that

$$C_v=C_v^0(T)+T\int_\infty^v\left(\frac{\partial^2 P}{\partial T^2}\right)_v dv \quad (A26)$$

and

$$\left(\frac{\partial C_v}{\partial T}\right)_v=\frac{dC_v^0}{dT}+\frac{\partial}{\partial T}\left[T\int_\infty^v\left(\frac{\partial^2 P}{\partial T^2}\right)_v dv\right]_v, \quad (A27)$$

the fundamental derivative of gasdynamics can be obtained analytically from an equation of state in the classical form $P=P(v,T)$ and by $C_v^0(T)$ or $C_p^0(T)$ as follows:

$$\Gamma=\frac{v^3}{2c^2}\left\{\left(\frac{\partial^2 P}{\partial v^2}\right)_T-3\frac{T}{C_v}\left(\frac{\partial P}{\partial T}\right)_v\left(\frac{\partial^2 P}{\partial v\,\partial T}\right)_{v,T}\right.$$
$$\left.+\left[\frac{T}{C_v}\left(\frac{\partial P}{\partial T}\right)_v\right]^2\left\{3\left(\frac{\partial^2 P}{\partial T^2}\right)_v+\frac{1}{T}\left(\frac{\partial P}{\partial T}\right)_v\left[1-\frac{T}{C_v}\left(\frac{\partial C_v}{\partial T}\right)_v\right]\right\}\right\}. \quad (A28)$$

Appendix B

Nonconventional Thermodynamic Functions for Computational Fluid Dynamics for Several Equations of State

1. PRSV Equations of State. The Peng-Robinson equation of state is

$$P=\frac{RT}{(v-b)}-\frac{a(T)}{v(v+b)+b(v-b)}. \quad (B1)$$

The parameter a introduced in the Styjeck-Vera modification of the PR EOS is given by

$$a(T)=a_c\times\alpha(T),$$

where

$$a_c=0.457235\frac{R^2T_c}{P_c},$$

$$\alpha(T)=[1+k(1-T_r^{0.5})]^2,$$

$$k=k_0+k_1(1+T_r^{0.5})(0.7-T_r)\ \text{ for }\ T_r<1;\ \ k_1=0\ \text{ for }\ T_r\geqslant 1,$$

$$k_0=0.378893+1.4897153\omega-0.17131848\omega^2+0.0196554\omega^3.$$

T_c is the critical temperature and $T_r=T/T_c$. k_1 is obtained from saturation-pressure fitting of experimental data or from fitting values to an accurate $P^{\text{sat}}=P(T^{\text{sat}})$ equation.

For a pure fluid the parameter b is not a function of temperature, while for a mixture, the mixing rules introduce a weak dependence on T. For this reason the pressure derivatives for a pure fluid differ from the mixtures ones.

The derivatives of P with respect to v at constant T is the same for pure fluids and multicomponent fluids:

$$\left(\frac{\partial P}{\partial v}\right)_T=\frac{-RT}{(b-v)^2}+\frac{2a(b+v)}{(v^2+2bv-b^2)}, \quad (B2)$$

$$\left(\frac{\partial^2 P}{\partial v^2}\right)_T=2\left(\frac{RT}{(v-b)^3}-\frac{a(3v^2+6vb+5b^2)}{(v^2+2vb-b^2)^3}\right). \quad (B3)$$

The derivatives of P with respect to T at constant v are different depending on the single-component or multicomponent case. For a pure fluid,

$$\left(\frac{\partial P}{\partial T}\right)_v=\frac{R}{(b-v)}+\frac{a'(T)}{(b^2-2bv-v^2)}, \quad (B4)$$

$$\left(\frac{\partial^2 P}{\partial T^2}\right)_v=-\frac{a''(T)}{b(v-b)+v(v+b)}, \quad (B5)$$

$$\left(\frac{\partial^2 P}{\partial v\,\partial T}\right)_{T,v}=-\frac{RT}{(v-b)^2}+2a'(T)\frac{2(v+b)}{(v^2+2vb-b^2)^2}. \quad (B6)$$

The derivatives of $a(T)$ are omitted for brevity. The integral for the real gas correction is given by

$$\int_\infty^v\left(\frac{\partial^2 P}{\partial T^2}\right)_v dv=a''(T)\frac{\text{Log}\left[\frac{z+(1+\sqrt{2})B}{Z+(1-\sqrt{2})B}\right]}{2\sqrt{2}b} \quad (B7)$$

with

$$Z=\frac{Pv}{RT};\ \ B=\frac{bRT}{P}. \quad (B8)$$

For the expression of $(\partial C_v/\partial T)_v$, it is useful to define

$$Y=\frac{Z+(1+\sqrt{2})B}{Z+(1-\sqrt{2})B}. \quad (B9)$$

The partial derivative of the specific heat with respect to T at constant v is given by

$$\left(\frac{\partial C_v}{\partial T}\right)_v=\frac{dC_v^0}{dT}+\frac{1}{2\sqrt{2}b}\text{Log}(Y)(Ta'''(T)+a''(T))$$
$$+\frac{T}{2\sqrt{2}bY}a''(T)\frac{\partial Y}{\partial T} \quad (B10)$$

with

$$\frac{\partial Y}{\partial T}=\frac{\partial Z/\partial T+(1+\sqrt{2})\partial B/\partial T}{Z-(\sqrt{2-1})B}$$
$$-\frac{[Z+(1+\sqrt{2})B][\partial Z/\partial T+(1-\sqrt{2})\partial B/\partial T]}{[Z-(\sqrt{2-1})B]^2}.$$

2 PRSV EOS and WS Mixing Rules. The WS mixing rules for the a and b parameters are given by

$$b_{\text{mixture}}=\frac{Q}{1-D}, \quad (B12)$$

$$a_{\text{mixture}}=RT\frac{QD}{1-D}, \quad (B13)$$

where

$$Q=\sum_i \sum_j x_i x_j \left(b-\frac{a}{RT}\right)_{i,j}, \tag{B14}$$

$$D=\sum_i x_i \frac{a_i}{b_i RT}+\frac{G^E_{P\to 0}}{RT}. \tag{B15}$$

In the above expression, a_i and b_i are the CEOS coefficients for the pure components and x_i are the mole fractions of the components. The excess Gibbs energy at low pressure, $G^E_{P\to 0}$, must be determined from a low pressure liquid activity coefficient model. The binary interaction parameter, k_{ij} contained in the combining rule

$$b_{ij}-\frac{a_{ij}}{RT}=\left[\left(b_i-\frac{a_i}{RT}\right)+\left(b_j-\frac{a_j}{RT}\right)\right]\frac{(1-k_{ij})}{2}, \tag{B16}$$

must be computed from the same liquid model.

The derivatives of P with respect to T at constant v for a multicomponent fluid are given by

$$\left(\frac{\partial P}{\partial T}\right)_v=\frac{RTb'(T)}{(b-v)^2}+\frac{R}{(b-v)}+\frac{a'(T)}{(b^2-2bv-v^2)}-\frac{2a(b-v)b'(T)}{(v^2+2bv-b^2)^2}, \tag{B17}$$

$$\left(\frac{\partial^2 P}{\partial T^2}\right)_v=\frac{2Rb'(T)}{(v-b)^2}+\frac{2RT(b'(T))^2}{(v-b)^3}+\frac{2a'(T)[vb'(T)+(v-b)b'(T)-bb'(T)]}{[(v-b)b+v(v+b)]^2}-\frac{a''(T)}{(v-b)b+v(v+b)}+\frac{RTb''(T)}{(v-b)^2}+\frac{a[-2(b'(T))^2+vb''(T)+(v-b)b''(T)-bb''(T)]}{[b(v-b)+v(v+b)]^2}, \tag{B18}$$

$$\left(\frac{\partial^2 P}{\partial v\,\partial T}\right)_{T,v}=-\frac{RT}{(v-b)^2}+\frac{2(v+b)a'(T)}{(v^2+2vb-b^2)^2}-\frac{2[a(v-b)^3(3v^2-2vb-3b^2)+RT(v^2+2vb-b^2)^3]b'(T)}{(v^3+v^2b-3vb^2+b^3)^3}. \tag{B19}$$

The temperature derivatives of the a and b parameters for the PRSV EOS and the WS mixing rules can be expressed as follows:

$$W_1=Q\cdot D+D\cdot T\cdot Q'(T)+D'(T)\cdot Q\cdot T, \tag{B20}$$

$$W_2=T\cdot Q\cdot D\cdot D'(T), \tag{B21}$$

$$W_3=1-D, \tag{B22}$$

$$b'(T)=\frac{W_1}{W_3}+\frac{W_2}{W_3^2}, \tag{B23}$$

$$a'(T)=R\left(\frac{W_1}{W_3}+\frac{W_2}{W_3^2}\right)=Rb'(T). \tag{B24}$$

The second temperature derivatives of a and b are omitted for brevity. They can be obtained in a similar way.

The derivatives of Q and D are given by

$$D'(T)=\sum_i x_i \frac{(-a_i+Ta_i'(T))}{b_i RT^2}-\frac{g^E_{\text{low}P}(x_i)}{\sigma RT^2}, \tag{B25}$$

$$Q'(T)=\sum_i \sum_j \frac{1}{2RT}\left(\frac{a_i+a_j}{T}-a_i'(T)-a_j'(T)\right)x_i x_j(1-k_{i,j}), \tag{B26}$$

$$D''(T)=\sum_i x_i\left[\frac{1}{b_i RT}a_i''(T)-\frac{2}{b_i RT^3}(Ta_i'(T)-a_i)\right]+\frac{g^E_{\text{low}P}(x_i)}{\sigma RT^3}, \tag{B27}$$

$$Q''(T)=\sum_i \sum_j \frac{1}{RT}\left[(a_i'(T)-a_j'(T))\frac{1}{T}-(a_i''(T)-a_j''(T))\frac{1}{2}-\frac{a_i+a_j}{T^2}\right]x_i x_j(1-k_{i,j}). \tag{B28}$$

By imposing that b does not depend on the temperature, the expression valid for pure fluids is obtained.

The integral for the real gas correction is given by

$$\int_\infty^v \left(\frac{\partial^2 P}{\partial T^2}\right)_v dv=-\frac{RT(b'(T))^2}{(b-v)^2}+\frac{R[2b'(T)+Tb''(T)]}{(b-v)}-\frac{2a(b'(T))^2(b-3v)}{(v^2+2bv-b^2)^2}+\frac{2bva'(T)b'(T)+(bvb''(T)-2b(b'(T))^2-2v(b'(T))^2)}{b^2(v^2+2bv-b^2)^2}+\frac{b^2a''(T)+2a(b'(T))^2-b[ab''(T)+2a'(T)b'(T)]}{2\sqrt{2}2b^3}\times\text{Log}\left[\frac{Z+(1+\sqrt{2})B}{Z+(1-\sqrt{2})B}\right]. \tag{B29}$$

For the computation of the fundamental derivative of gas dynamics, the partial derivative $(\partial C_v/\partial T)_v$ must also be computed. This derivative involves, furthermore, the computation of $a'''(T)$, $b'''(T)$. In this case the use of a software for automated symbolical computation is mandatory and the resulting expressions are omitted for brevity.

3 Starling EOS. The Starling EOS is in the form

$$P=\rho RT+\left(B_0RT-A_0-\frac{C_0}{T^2}+\frac{D_0}{T^3}+\frac{E_0}{T^4}\right)\rho^2+\left(bRT-a-\frac{b}{T}\right)\rho^3+\alpha\left(a+\frac{d}{T}\right)\rho^6+c\frac{\rho^3}{T^2}(1+\theta\rho^2)e^{-\theta\rho^2}. \quad (B30)$$

All thermodynamic functions can be expressed starting from the following expressions:

$$\left(\frac{\partial P}{\partial v}\right)_T=-\frac{RT}{v^2}-2\frac{B_0RT-A_0-\frac{C_0}{T^2}+\frac{D_0}{T^3}-\frac{E_0}{T^4}}{v^3}-3\frac{bRT-a-\frac{d}{T}}{v^4}-6\frac{\alpha\left(a+\frac{d}{T}\right)}{v^7}-3\frac{c\left(1+\frac{\theta}{v^2}\right)e^{-\theta/v^2}}{v^4T^2}-2\frac{c\theta e^{-\theta/v^2}}{v^6T^2}+2\frac{c\left(1+\frac{\theta}{v^2}\right)\theta e^{-\theta/v^2}}{v^6T^2}, \quad (B31)$$

$$\left(\frac{\partial P}{\partial T}\right)_v=\frac{T}{v}+\frac{B_0R+2\frac{C_0}{T^3}-3\frac{D_0}{T^4}+4\frac{E_0}{T^5}}{v^2}+\frac{bR-\frac{d}{T^2}}{v^3}-\frac{\alpha d}{T^2v^6}-2\frac{c\left(1+\frac{\theta}{v^2}\right)e^{-\theta/v^2}}{v^3T^3}, \quad (B32)$$

$$\left(\frac{\partial^2 P}{\partial T^2}\right)_v=\frac{-6\frac{C_0}{T^4}+12\frac{D_0}{T^5}-20\frac{E_0}{T^6}}{v^2}-\frac{2d}{T^3v^3}+\frac{2\alpha d}{T^3v^6}+6\frac{c\left(1+\frac{\theta}{v^2}\right)e^{-\theta/v^2}}{v^3T^4}, \quad (B33)$$

$$\left(\frac{\partial^2 P}{\partial v^2}\right)_T=2\frac{RT}{v^3}+6\frac{B_0RT-A_0-\frac{C_0}{T^2}+\frac{D_0}{T^3}-\frac{E_0}{T^4}}{v^4}+12\frac{bRT-a-\frac{d}{T}}{v^5}+42\frac{\alpha\left(a+\frac{d}{T}\right)}{v^8}+12\frac{c\left(1+\frac{\theta}{v^2}\right)e^{-\theta/v^2}}{v^5T^2}+18(1-\theta)\frac{c\theta e^{-\theta/v^2}}{v^7T^2}-\left(1+\frac{\theta}{v^2}\right)\frac{4ce^{-\theta/v^2}}{v^9T^2}\theta, \quad (B34)$$

$$\left(\frac{\partial^2 P}{\partial v\,\partial T}\right)_{T,v}=-\frac{R}{v^2}-\frac{2}{v^3}\left(B_0R+\frac{2C_0}{T^3}-\frac{3D_0}{T^4}+\frac{4E_0}{T^5}\right)-\frac{3}{v^4}\frac{\alpha d}{T^2v^7}+\frac{6}{v^4T^3}\left(1+\frac{\theta}{v^2}\right)e^{-\theta/v^2}-\frac{4}{v^6T^3}c\theta e^{-\theta/v^2}\frac{\theta}{v^2}, \quad (B35)$$

$$\int_\infty^v\left(\frac{\partial^2 P}{\partial T^2}\right)_v dv=-\frac{6c}{\theta T^4}+\frac{e^{-\theta/v^2}}{5\theta T^6v^5}(30v^4C_0T^2\theta e^{\theta/v^2}-60v^4D_0T\theta e^{\theta/v^2}+100v^4E_0\theta e^{\theta/v^2}+5dT^3v^3\theta e^{\theta/v^2}-2\alpha dT^3\theta e^{\theta/v^2}+30cT^2v^5+15cT^2v^3\theta). \quad (B36)$$

The expression for $(\partial C_v/\partial T)_v$ is omitted because it is too lengthy.

4 Martin-Hou EOS. The Martin-Hou EOS is in the form

$$P=\frac{RT}{v-b}+\sum_{i=2}^{5}\frac{1}{(v-b)^i}(A_i+B_iT+C_ie^{-kT/T_C})+\frac{A_6+B_6T+C_6e^{-kT/T_C}}{e^{\alpha v}(1+ce^{\alpha v})}. \quad (B37)$$

All thermodynamic functions can be expressed starting from the following expressions:

$$\left(\frac{\partial P}{\partial v}\right)_T=-\frac{Rt}{(v-b)^2}-\sum_{i=2}^{5}\frac{i}{(v-b)^{i+1}}(A_i+B_iT+C_ie^{-kT/T_C})-\frac{\alpha(A_6+B_6T+C_6e^{-kT/T_C})}{e^{\alpha v}}, \quad (B38)$$

$$\left(\frac{\partial P}{\partial T}\right)_v=\frac{RT}{v-b}+\sum_{i=2}^{5}\frac{1}{(v-\mathbf{n})^i}\left(B_i-\frac{C_ike^{-kT/T_C}}{T_C}\right)+\frac{1}{e^{\alpha v}}\left(B_6-\frac{C_6ke^{-kT/T_C}}{T_C}\right), \quad (B39)$$

$$\left(\frac{\partial^2 P}{\partial T^2}\right)_v=\sum_{i=2}^{5}\frac{1}{(v-b)^i}\left(\frac{C_ik^2e^{-kT/T_C}}{T_C^2}\right)+\frac{C_6k^2e^{-kT/T_C}}{T_C^2e^{\alpha v}}, \quad (B40)$$

$$\left(\frac{\partial^2 P}{\partial v^2}\right)_T=2\frac{RT}{(v-b)^3}+\sum_{i=2}^{5}\frac{i^2+i}{(v-b)^{i+2}}(A_i+B_iT+C_ie^{-kT/T_C})+\alpha^2\frac{A_6+B_6T+C_6e^{-kT/T_C}}{e^{\alpha v}}, \quad (B41)$$

$$\left(\frac{\partial^2 P}{\partial v\,\partial T}\right)_{T,v}=-\frac{RT}{(v-b)^2}-\sum_{i=2}^{5}\frac{i}{(v-b)^{i+1}}\left(B_i-\frac{C_ike^{-kT/T_C}}{T_C}\right)-\frac{\alpha}{e^{\alpha v}}\left(B_6-\frac{C_6ke^{-kT/T_C}}{T_C}\right), \quad (B42)$$

$$\left(\frac{\partial^2 P}{\partial T^2}\right)_v=\sum_{i=2}^{5}\frac{1}{(v-b)^i}\left(\frac{C_ik^2e^{-kT/T_C}}{T_C^2}\right)+\frac{C_6k^2e^{-kT/T_C}}{T_C^2e^{\alpha v}}, \quad (B43)$$

$$\int_\infty^v\left(\frac{\partial^2 P}{\partial T^2}\right)_v dv=-\frac{1}{12}k^2[(12C_2v^3-36C_2v^2b+36C_2vb^2-12C_3b^3+6C_3v^2-12C_3vb+6C_3b^2+4C_4v-4C_4b+3C_5)e^{\alpha v}\alpha+12C_6v^4-48C_6v^3b+72C_6v^2b^2-48C_6vb^3+12C_6b^4]\frac{e^{(-kT+v\alpha T_C/T_C)}}{[(b-v)^4T_C^2\alpha]}. \quad (B44)$$

Note that the above expression is valid if $\alpha>0$ or $\alpha=0$ and $C_6=0$. This is verified for all fluids in the TPSI database. The expression for $(\partial C_v/\partial T)_v$ is omitted for brevity.

References

[1] Wagner, B., and Schmidt, W., 1978, ''Theoretical Investigation of Real Gas Effects in Cryogenic Wind Tunnels,'' AIAA J., **16**, pp. 580–586.

[2] Anderson, W. K., May 1991, ''Numerical Study of the Aerodynamic Effects of Using Sulfur Hexafluoride as a Test Gas in Wind Tunnels,'' NASA Technical Paper 3086, NASA Langley Research Center, Hampton, VA.

[3] Anders, J. B., Anderson, W. K., and Murthy, A. V., 1999, ''Transonic Similarity Theory Applied to a Supercritical Airfoil in Heavy Gases,'' J. Aircr., **36**, Nov–Dec, pp. 957–964.

[4] Korte, J. J., 2000, ''Inviscid Design of Hypersonic Wind Tunnel Nozzles for Real Gas,'' E. Camhi, ed., *Proceedings of the 38th Aerospace Sciences Meeting and Exhibit*, Reno, NV, Jan. 10–13, AIAA, Reston, VA, pp. 1–8.

[5] Bober, W., and Chow, W. L., 1990, ''Nonideal Isentropic Gas Flow Through Converging-Diverging Nozzles,'' ASME J. Fluids Eng., **112**, pp. 455–460.

[6] Dziedzidzic, W. M., Jones, S. C., Gould, D. C., and Petley, D. H., 1993, ''Analytical Comparison of Convective Heat Transfer Correlation in Supercritical Hydrogen,'' J. Thermophys. Heat Transfer, **7**, pp. 68–73.

[7] Brown, B. P., and Argrow, B. M., 2000, ''Application of Bethe-Zel'dovic-Thompson Fluids in Organic Rankine Cycle Engines,'' J. Propul. Power., **16** Nov–Dec, pp. 1118–1123.

[8] Angelino, G., and Colonna, P., 1998, ''Multicomponent Working Fluids for Organic Rankine Cycles (ORCs),'' Energy, **23**, pp. 449–463.

[9] Schnerr, G. H., and Leidner, P., 1993, ''Numerical Investigation of Axial Cascades for Dense Gases.'' E. L. Chin, ed., *PICAST'1—Pacific International Conference on Aerospace Science Technology*, Vol. 2, National Cheng Kung University, Publ., Taiwan, pp. 818–825.

[10] Monaco, J. F., Cramer, M. S., and Watson, L. T., 1997, ''Supersonic Flows of Dense Gases in Cascade Configurations,'' J. Fluid Mech., **330**, pp. 31–59.

[11] Angelino, G., and Invernizzi, C., 1996, ''Potential Performance of Real Gas Stirling Cycles Heat Pumps,'' Int. J. Refrig., **19**, p. 390.

[12] Angelino, G., and Invernizzi, C., 2000, ''Real Gas Effects in Stirling Engines,'' *35th Intersociety Energy Conversion Engineering (IECEC)*, Las Vegas, NV July, AIAA, Reston, VA, pp. 69–75.

[13] Fitzgerald, R., 1999, ''Traveling Waves Thermoacustic Heat Engines Attain High Efficiency,'' Phys. Today, **52**, pp. 18–20.

[14] Glaister, P., 1988, ''An Approximate Linearized Riemann Solver for the Euler Equations for Real Gases,'' J. Comput. Phys., **74**, pp. 382–408.

[15] Grossmann, B., and Walters, R. W., 1989, ''Analysis of the Flux-Split Algorithms for Euler's Equations With Real Gases,'' AIAA J., **27**, pp. 524–531.

[16] Vinokur, M., and Montagne', J. L., 1990, ''Generalized Flux-Vector Splitting and Roe Average for an Equilibrium Real Gas,'' J. Comput. Phys., **89**, pp. 276–300.

[17] Liou, M.-S., van Leer, B., and Shuen, J.-S., 1990, ''Splitting of Inviscid Fluxes for Real Gases,'' J. Comput. Phys., **87**, pp. 1–24.

[18] Mottura, L., Vigevano, L., and Zaccanti, M., 1997, ''An Evaluation of Roe's Scheme Generalizations for Equilibrium Real Gas Flows,'' J. Comput. Phys., **138**, pp. 354–339.

[19] Guardone, A., Selmin, V., and Vigevano, L., 1999, ''An Investigation of Roe's Linearization and Average for Ideal and Real Gases,'' Scientific Report DIA-SR 99-01, Politecnico di Milano, Dipartimento di Ingegneria Aerospaziale, Jan.

[20] Drikakis, D., and Tsangaris, S., 1993, ''Real Gas Effects for Compressible Nozzle Flows,'' ASME J. Fluids Eng., **115**, pp. 115–120.

[21] Cravero, C., and Satta, A., 2000, ''A CFD Model for Real Gas Flows,'' ASME Turbo Expo, Munich, May, ASME, New York, pp. 1–10.

[22] Aungier, R. H., 1995, ''A Fast, Accurate Real Gas Equation of State for Fluid Dynamic Analysis Applications,'' ASME J. Fluids Eng., **117**, pp. 277–281.

[23] Cramer, M. S., 1991, *Nonclassical Dynamics of Classical Gases* (Nonlinear Waves in Real Fluids) International Center for Mechanical Sciences, Courses and Lectures, Springer-Verlag, Berlin.

[24] Aldo, A. C., and Argrow, B. M., 1994, ''Dense Gas Flows in Minimum Lenght Nozzles,'' ASME J. Fluids Eng., **117**, pp. 270–276.

[25] Argrow, B. M., 1996, ''Computational Analysis of Dense Gas Shock Tube Flow,'' Shock Waves, **6**, pp. 241–248.

[26] Brown, B. P., and Argrow, B. M., 1998, ''Nonclassical Dense Gas Flows for Simple Geometries,'' AIAA J., **36**, (Oct) pp. 1842–1847.

[27] Brown, B. P., and Argrow, B. M., 1997, ''Two-Dimensional Shock Tube Flow for Dense Gases,'' J. Fluid Mech., **349**, pp. 95–115.

[28] Cramer, M. S., and Park, S., 1999, ''On the Suppression of Shock-Induced Separation in Bethe-Zel'dovich-Thompson Fluids,'' J. Fluid Mech., **393**, pp. 1–21.

[29] Colonna, P., Rebay, S., and Silva, P., 2002, ''Computer Simulations of Dense Gas Flows Using Complex Equations of State for Pure Fluids and Mixtures and State of the Art Numerical Schemes,'' Tech Report Università di Brescia, Brescia, Italy.

[30] Reynolds, W. C., 1979, ''Thermodynamic Properties in S.I.,'' Department of Mechanical Engineering, Stanford University, Stanford, CA.

[31] Sandler, S. I., et al., 1994, *Models for Thermodynamic and Phase Equilibria Calculations*, Marcel Dekker, New York.

[32] Span, R., Wagner, W., Lemmon, E. W., and Jacobsen, R. T., 2001, ''Multiparameter Equations of State—Recent Trends and Future Challanges,'' Fluid Phase Equilib., **183–184**, pp. 1–20.

[33] Smith, D. H., and Fere, M., 1995, ''Improved Phase Boundary for One-Component Vapor-Liquid Equilibrium Incorporating Critical Behavior and Cubic Equations of State,'' Fluid Phase Equilib., **113**, pp. 103–115.

[34] Wong, D. S. H., and Sandler, S. I., 1993, ''A Theoretically Correct Mixing Rule for Cubic Equations of State,'' AIChE J., **38**, pp. 671–680.

[35] Keenan, J. H. et al., 1969, *Steam Tables*, John Wiley and Sons, New York.

[36] Haar, L., and Gallagher, J. S., 1978, ''Thermodynamics Properties of Ammonia,'' J. Phys. Chem. Ref. Data, **7**, pp. 635–791.

[37] Starling, K. E., 1973, *Equation of State and Computer Prediction—Fluid Thermodynamic Properties for Light Petroleum Substances* Gulf Publishing, Houston.

[38] Martin, J. J., and Hou, Y. C., 1955, ''Development of an Equation of State for Gases,'' AIChE J., **1** (June), pp. 142–151.

[39] McLinden, M. O., Lemmon, E. W., and Jacobsen, R. T., 1998, ''Thermodynamic Properties for the Alternative Refrigerants,'' Int. J. Refrig. , **21** (June), pp. 322–338.

[40] Stryjeck, R., and Vera, J. H., 1986, ''PRSV: An Improved Peng-Robinson Equation of State for Pure Compounds and Mixtures,'' Can. J. Chem. Eng., **64**, pp. 323–333.

[41] Prausnitz, J. M., 1995, ''Some New Frontiers in Chemical Engineering Thermodynamics,'' Fluid Phase Equilib., **104**, pp. 1–20.

[42] Bassi, F., Rebay, S., and Savini, M., 1991, ''Transonic and Supersonic Inviscid Computations in Cascades Using Adaptive Unstructured Meshes,'' International Gas Turbine & Aeroengine Congress & Exhibition, Orlando, FL., June 3–6, ASME, New York.

[43] Rebay, S., 1992, ''Soluzione Numerica Adattiva su Reticoli non Strutturati delle Equazioni di Eulero,'' Ph.D. thesis, Politecnico di Milano, Milano.

[44] Taylor, R., 1997, ''Automatic Derivation of Thermodynamic Property Functions Using Computer Algebra,'' Fluid Phase Equilib., **129**, pp. 37–47.

[45] Press, W. H., Teukolsky, S. A., Vetterling, W. T., and Flannery, B. P., 1993, *Numerical Recipes in Fortran 77: The Art of Scientific Computing* (Vol. 2, Numerical Analysis Series), 2nd Ed., Cambridge University Press, Cambridge, UK.

[46] Lemmon, E. W., McLinden, M. O., and Friend, D. G., 2001, Thermophysical Properties of Fluid Systems (NIST Chemistry WebBook, NIST Standard Reference Database Number 69), National Institute of Standards and Technology, Gaithersburg MD.

[47] Moldover, M., Mehl, J. B., and Greenspan, M., 1986, ''Gas-Filled Spherical Resonators: Theory and Experiment,'' J. Acoust. Soc. Am., **79**, pp. 253–272.

[48] Cramer, M. S., November 1989, ''Negative Nonlinearity in Selected Fluorocarbons,'' Phys. Fluids A, **11**, pp. 1894–1897.

[49] Thompson, P. A., and Lambrakis, K. C., 1973, ''Negative Shock Waves,'' J. Fluid Mech., **60**, pp. 187–208.

[50] Wilcock, D. F., 1946, ''Vapor Pressure-Viscosity relations in Methylpolysiloxanes,'' J. Chem. Am. Soc., **68** (Apr) pp. 691–696.

[51] Colonna, P., 1996, ''*Fluidi di Lavoro Multi Componenti Per Cicli Termodinamici di Potenza*,'' Ph.D. thesis, Politecnico di Milano, Milano.

[52] Kalina, A. L., 1984, ''Combined Cycle Systems With Novel Bottoming Cycle,'' ASME J. Eng. Gas Turbines Power, **106**, pp. 737–742.

[53] Ibrahim, M. B., and Kovach, R. M., 1993, ''A Kalina Cycle Application for Power Generation,'' Energy, **18**, pp. 961–969.

[54] Marston, C. H., and Hyre, M., 1995, ''Gas Turbine Bottoming Cycles: Triple-Pressure Steam Versus Kalina,'' ASME J. Eng. Gas Turbines Power, **117**, pp. 10–15.

[55] Marston, C. H., 1990, ''Parametric Analysis of the Kalina Cycle,'' ASME J. Eng. Gas Turbines Power, **112**, pp. 107–116.

[56] Rogdakis, E. D., 1996, ''Thermodynamic Analysis, Parametric Study and Optimum Operation of the Kalina Cycle,'' Int. J. Energy Res., **20**, pp. 359–370.

[57] Heppenstall, T., 1998, ''Advanced Gas Turbine Cycles for Power Generation: A Critical Review,'' Appl. Therm. Eng., **18**, pp. 837–846.

[58] Verschoor, M. J. E., and Brouwer, E. P., 1995, ''Description of the SMR Cycle Which Combines Fluid Elements of Steam and Organic Rankine Cycles,'' Energy, **20**, p. 295.

[59] Orbey, H., and Sandler, S. I., 1995, ''Equation of State Modeling of Refrigerant Mixtures,'' Ind. Eng. Chem. Res., **34**, pp. 2520–2525.

[60] Lambrakis, K. C., and Thompson, P. A., 1972, ''Existence of Real Fluids With Negative Fundamental Derivative,'' Phys. Fluids, **15**, pp. 933–935.

[61] Flaningam, O. L., 1986, ''Vapor Pressures of Poly(Dimethylsiloxane) Oligomers,'' J. Chem. Eng. Data, **31**, pp. 266–272.

[62] Wagner, W., and Pruss, A., 2001, ''New International Formulation for the Thermodynamic Properties of Ordinary Water Substance for General and Scientific Use,'' J. Phys. Chem. Ref. Data, **30**, to be published.

[63] Span, R., 2000, *Multiparameter Equations of State—An Accurate Source of Thermodynamic Property Data*, Springer-Verlag, Berlin.

[64] Grigiante, M., Scalabrin, G., Benedetto, G., Gavioso, R. M., and Spagnolo, R., 2000, ''Vapor Phase Acoustic Measurements for R125 and Development of a Helmholtz Free Energy Equation,'' Fluid Phase Equilib., **174**, pp. 69–79.